Chapter 3

A Gain-Enhanced Slotted Patch Antenna Using Metasurface as Superstrate Configuration

3.1. Introduction

In the last chapter, the antenna performances have been improved by using the metasurface (MS) with the partial ground on the same dielectric. The impedance bandwidth of that structure has been improved after using 4×5 order MS with the slotted patch. The antenna exhibits an almost omnidirectional radiation pattern in the lower frequency band while at higher frequency, slight degradation in the radiation profile is noted. This may be due to leakage of out of phase fields from few slots either in the ground plane or at the patch.

In this chapter, a portable, directive and highly efficient MS-based fractal patch antenna has been discussed in which the slotted radiating patch and the MS are arranged in a stacked manner. Fractal geometrics accompanied by dielectric via have been integrated into the patch to shift the frequency of operation in the desired frequency region [116-118]. The shunt inductive effect dielectric via reduces the electric field around it. As a result, the field distribution is strongly perturbed that leads to tune-up of its resonant frequency, resulting in an increase in the electrical length of the patch and enhancing the radiation directivity. The optimal position of via in the middle line of the patch also improves the reflection coefficient

[116-118]. The defected ground concept has been used in the proposed prototype by incorporating two rectangular slots in the ground plane. This results in the reduction of surface waves that minimizes the cross-polarized radiation [122-123]. Moreover, the impedance bandwidth with co- to cross-polarized radiation characteristics in the broadside direction have been improved due to slot in microstrip patch [127-129]. Further, the antenna gain has been increased by introducing a 5×5 order metasurface acting as a superstrate to the patch. Here, the geometries of the MS structure arranged in a superstrate manner are able to control the resonant effects of the incident electromagnetic wave [112-113]. The MS designs in planar, as well as non-planar configurations, usually provide high impedance surfaces which can modulate the electromagnetic fields excited by a patch resonator [113-115].

The prototype has been analyzed using Ansys HFSS [126] and it affords a satisfactory return loss of 24 dB at 10.44 GHz. Furthermore, the designed prototype operates at the frequency band of 10.14-10.94 GHz with fractional bandwidth of 7.6%. The massive gain of 8.17 dBi with unidirectional radiation characteristics has been accomplished at 10.44 GHz after the incorporation of the MS design. The prototype of the proposed structure has been fabricated followed by experimental characterization. It is identified that the simulated and experimental results are in good agreement.

3.2. Design of the Antenna

The perspective antenna accumulates with a square patch arranged in a fractal manner where dielectric via is right at the center of the patch and an array of square patches are organized in a regular manner on the overhead of the patch. Dual rectangular-shaped slots have been established on the ground surface to enhance the impedance bandwidth of the antenna.

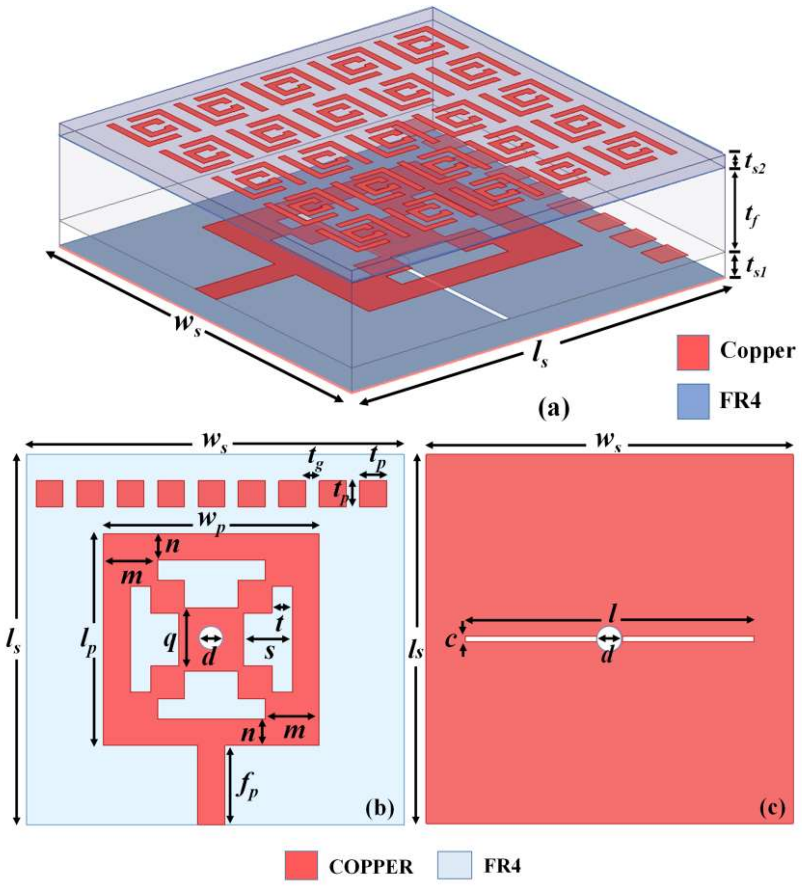

Fig. 3.1. (a) Three dimensional geometry of proposed structure with (b) top view of conventional patch and (c) rear view of conventional patch (Designed optimized parameters: w_s = 28 mm, l_s = 28 mm, t_{s1} = 1.6 mm, t_f = 6 mm, t_{s2} = 0.8 mm, l_p = 16 mm, w_p = 16 mm, q = 4.8 mm, s = 3.6 mm, n = 2 mm, m = 4 mm, f_p = 6 mm, t = 1.5 mm, t_g = 1 mm, t_p = 2 mm, c = 0.4 mm, d = 2 mm, l_1 = 10 mm).

The primary radiating element and the bottom layer of the antenna are separated by a 1.6 mm thick FR4 dielectric layer (loss tangent = 0.025 and relative permittivity = 4.4). An MS has been used in the structure by combining a periodic arrangement of unit cells where the unit cell is composed of a concentric C-type patterned patch surrounded by a couple of L-type patterned patches at the outer boundary to significantly improve the gain of the antenna. The MS layer is also organized on FR4 dielectric having 0.8 mm thickness. Moreover, the

conventional patch and the MS layer have been separated by a 6 mm thick Teflon dielectric (loss tangent = 0.001 and relative permittivity = 2.1).

The optimized geometrical dimensions of the three-dimensional structure together with top and rear views of the conventional antenna are represented in Fig. 3.1(a), Fig. 3.1(b) and Fig. 3.1(c) respectively. A 50Ω microstrip feed-line has been fed into this antenna using an SMA connector through the substrate and ground layer. The designed antenna works in the X-band region in which the operational band can be tuned by just adjusting the location of dielectric via and dimensions of the periodic slots. The designed evolution of the conventional patch antenna with four different steps has been illustrated graphically in Fig. 3.2. The corresponding return loss responses have been represented in Fig. 3.3. For further study, parametric studies are performed to identify the effects of various parameters in terms of impedance bandwidth and return loss.

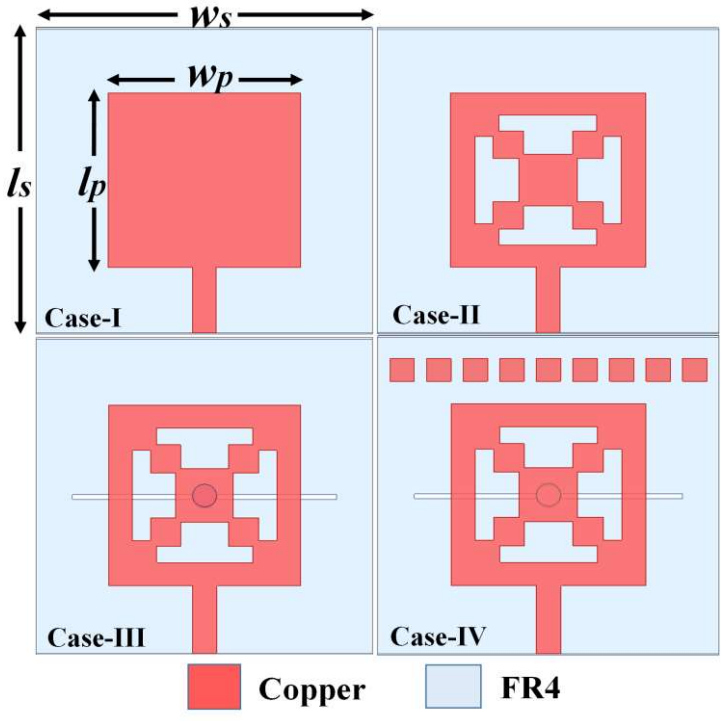

Fig. 3.2. Design steps of the conventional patch with different modifications.

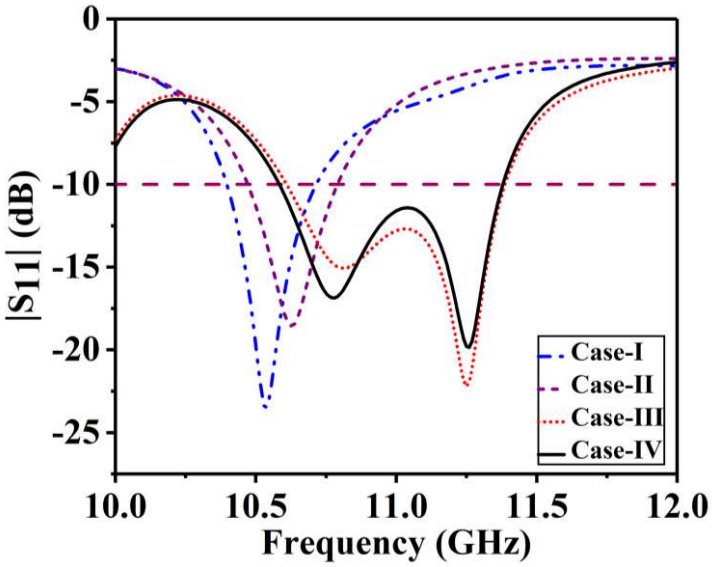

Fig. 3.3. The plot of $|S_{11}|$ (dB) with respect to frequency (GHz) for various modified antennas as specified in Fig. 3.2.

3.2.1. Fractal Slotted Patch

In the beginning, a conventional microstrip patch antenna has been patterned on a 1.6 mm thick low-cost FR4 substrate which is performing a narrow impedance bandwidth with low gain. Next, the microstrip patch has reformed into a fractal shape by etching four different fractal square-shaped slots as highlighted in Case-I of Fig. 3.2.

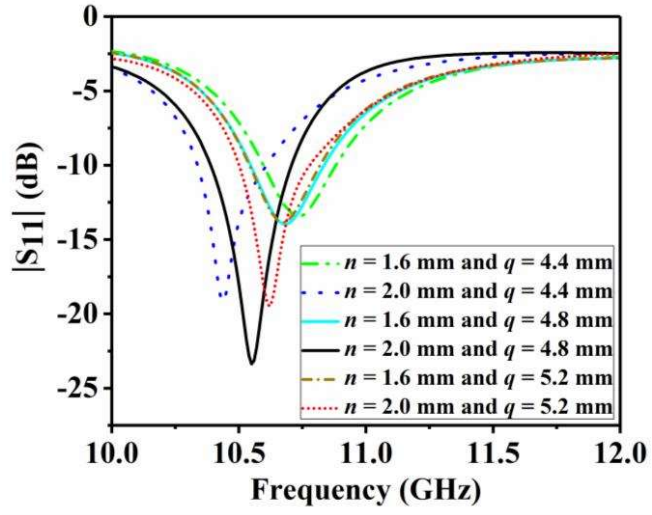

Fig. 3.4. The plot of $|S_{11}|$ (dB) with respect to frequency for *n*- and *q*-variations.

The effect of the centre patch length (q) and outer side interface thickness (n) are presented in Fig. 3.4. It has been observed that n = 2 mm along with q = 4.8 mm exhibits good impedance matching. Here, the gap t and s directly depend upon the centre patch length (q). After the optimization of the length and width of the slots, the antenna gain has been increased to 5.3 dBi accompanied by impedance bandwidth of 3.02% at 10.54 GHz operating frequency.

3.2.2. Introduction of Dielectric Via

A 2 mm diameter dielectric via has been placed appropriately at the center by tuning the operating frequencies of fractal patch represented as Case-II of Fig. 3.2. It has been observed that the impedance bandwidth remains invariant with respect to the diameter of the dielectric via (d) illustrated in Fig. 3.5. This improves the antenna's effective permittivity and contributes towards the miniaturization of the patch antenna [66-67]. Here the antenna operates at the frequency of 10.6 GHz with almost identical fractional bandwidth and realized gain of 6.99 dBi.

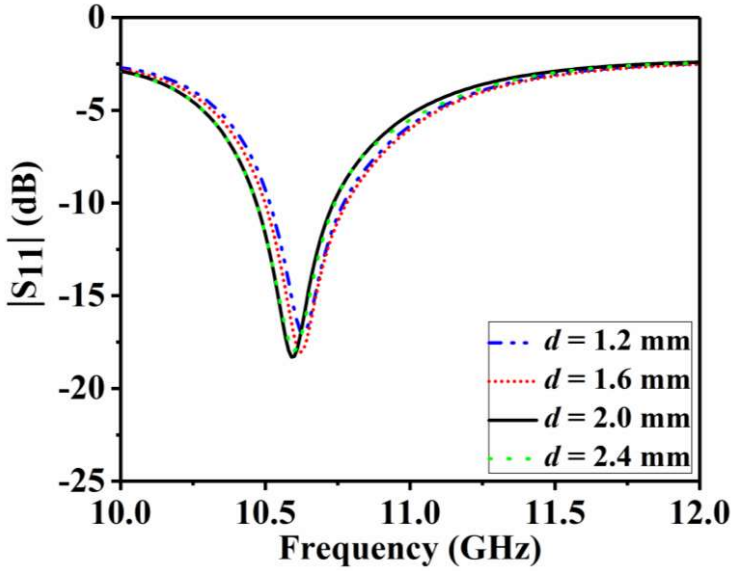

Fig. 3.5. The plot of $|S_{11}|$ (dB) with respect to the frequency at d-variations.

3.2.3. Addition of Rectangular Slots and Dielectric Via in the Ground Layer

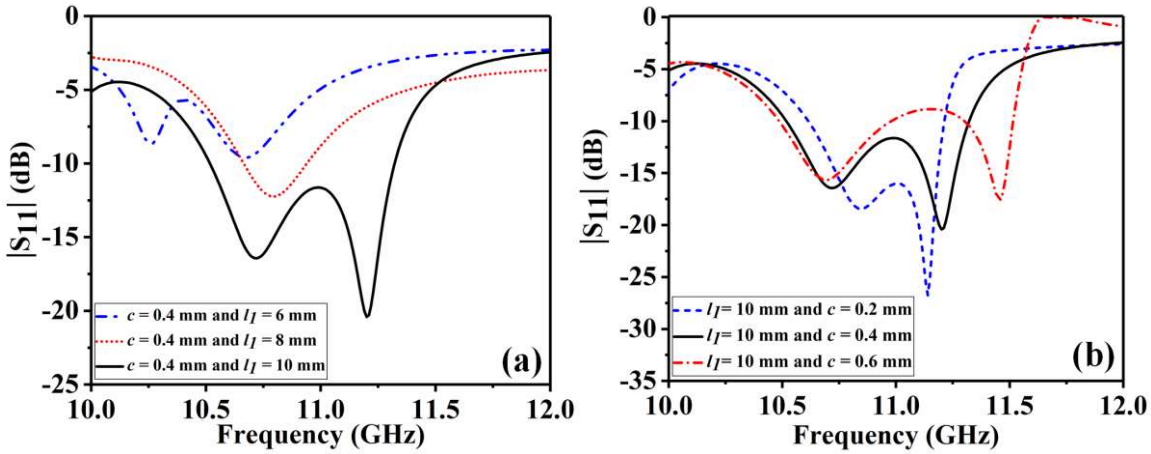

Fig. 3.6. Plot of $|S_{11}|$ (dB) with respect to frequency (a) at constant c = 0.4 mm and l_1 variations (b) at constant l_1 = 10 mm and c variations.

The rectangular slots in the ground layer and dielectric via at the center are simultaneously unified into the patch in Case-III of Fig. 3.2. In this arrangement, Fig. 3.6 demonstrates the effect of the ground plane slot width (c) and slot length (l_1) in terms of impedance bandwidth and return loss. The slots in the ground plane behave as a load introduced to the antenna which can be used to bring the input impedance closer to the characteristic impedance (50 ohms). This improves the input impedance match and hence the reflection characteristics ($|S_{11}|$). The slots are placed in such a way that it can reduce the radiation, hence the effect of the slot can be represented by a purely reactive impedance. The slot input impedance affects differently depending on the antenna geometry and the position of the slot. The two 0.4×10 mm^2 rectangular slots are etched from the ground plane which results in the improvement of the impedance bandwidth to 6.2% at 11.24 GHz whereas the gain has been reduced to 5.91 dBi. So it is found that impedance bandwidth enhancement takes place due to the defected ground structure [127-129]. Further, the combining effects of the parameters l_1, c, and d are mentioned in Fig. 3.7. Here the antenna shifts the fundamental resonant frequency to the

higher frequency side which operates at 10.82 GHz with a maximum bandwidth of 7.2% and gain of 5.22 dBi.

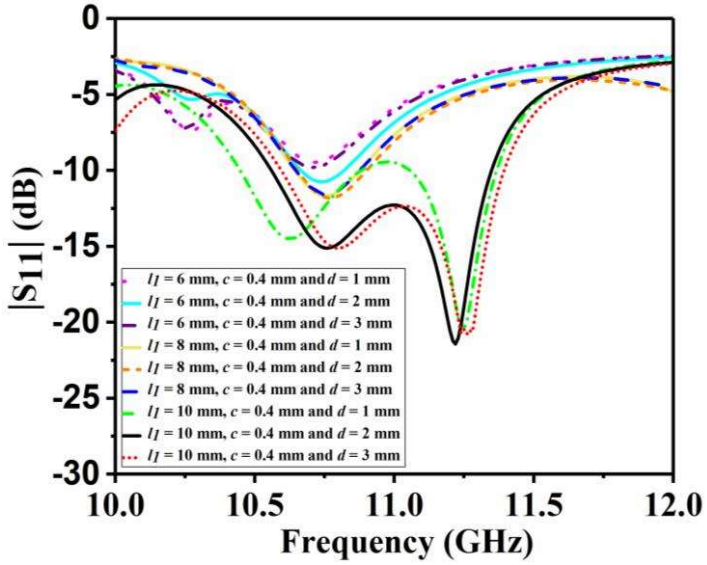

Fig. 3.7. The plot of $|S_{11}|$ (dB) with respect to the frequency at l_1, c and d-variations.

3.2.4. Inclusion of Array of Square Patches

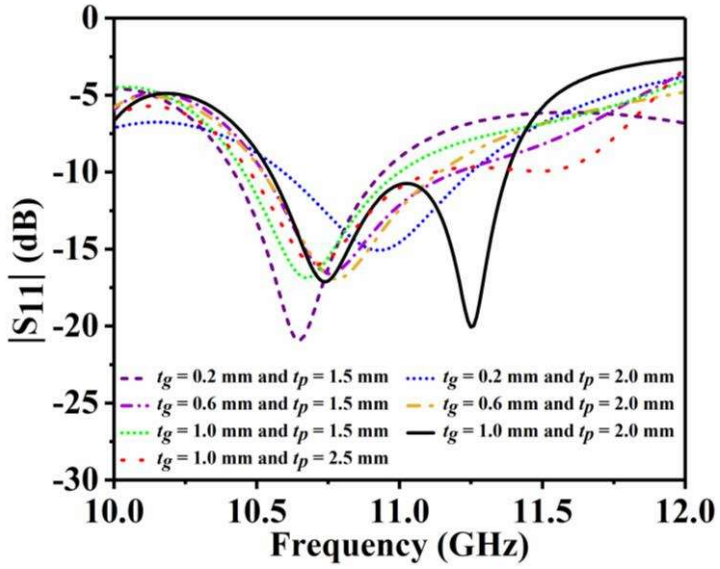

Fig. 3.8. The plot of $|S_{11}|$ (dB) with respect to the frequency at t_g and t_p variations.

Later, in Case-IV of Fig. 3.2, a 1×9 array of square patches have been integrated on the upper region of the fractal patch, and the parametric study of the gap between small square patch (t_g) and patch dimension (t_p) are mentioned in Fig. 3.8. Here, the square patch is optimized to 2×2 mm^2 and the patches are mutually separated by 1 mm. This array of patches enhances the fractional bandwidth to 7.26% at 11.28 GHz while 5.90 dBi of optimum gain has been achieved at 10.78 GHz. Here, each square patch is inductive and the gap between the two square patches provides the capacitive response. The 1×9 array of the square patches forms a cascaded form of the LC circuit. Since each LC circuit resonates at a specific frequency, the combination of the cascaded LC network and the fractal patch (which forms another LC circuit) makes the complete equivalent circuit. The equivalent input impedance of the square patches can be expressed as the cascaded network of the impedances of the periodic pattern and the grounded dielectric layer impedance. This results in the equality between the fractal patch bandwidth and the bandwidth of a parallel LC circuit with net inductance and capacitance of L_p and C_p, respectively as seen in (2.1),

$$BW=\frac{\omega_0^2 L_{mp}}{Z_0}=\frac{1}{C_{mp}Z_0} \tag{2.1}$$

where Z_0 is the free space impedance. This implies that by lowering C_p, the patch bandwidth can also be enhanced, which can be accomplished by forming a slot gap between the central patch and the rectangular strips. The etched slot gap between the central patch and the rectangular strips generates a capacitive effect, and the series combination of these capacitances reduces the total equivalent capacitance of the device, thereby improving the reflection bandwidth to 7.26%. Due to the aforementioned performance enhancement, this

antenna has been considered as the conventional patch antenna for different device applications.

3.2.5. Design of the Metasurface

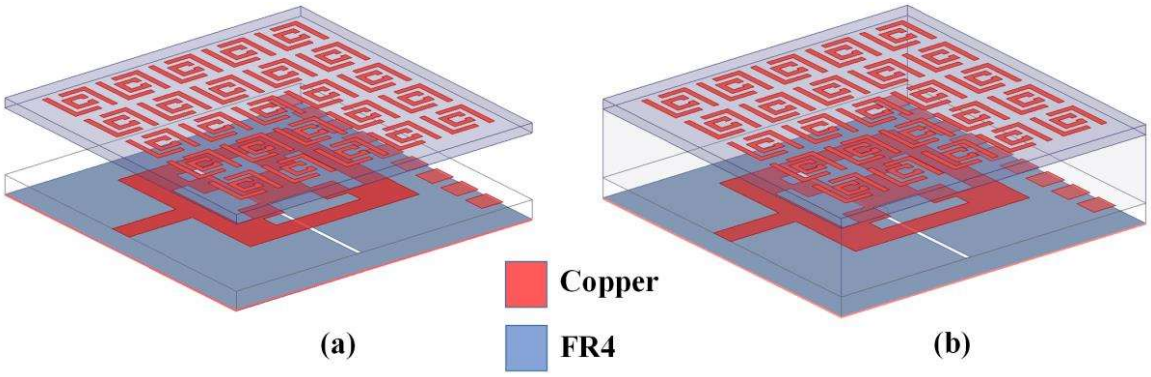

Fig. 3.9. Design of structure with (a) air spacer and (b) Teflon dielectric in between two FR4 substrates.

The performance of the conventional patch antenna depicted as Case IV of Fig. 3.2 has been enhanced by the inclusion of MS as a superstrate configuration. The MS layer has been accumulated over a 0.8 mm thick FR4 dielectric lying above the conventional patch antenna. Initially, the MS layer is separated from the conventional patch by air spacer further it is replaced by Teflon dielectric (relative permittivity of 2.1). Initially, the single-layer slotted patch antenna is propagating in TM_{01} mode. TM_{01} excitation is highest with the least power coupling at a specified feed position. After incorporating the MS with the patch in a superstrate configuration, the structure is propagating in TM_{03} mode. The TM_{03} modal amplitude is very high with respect to the other modes at the chosen feed location. The antenna configuration with air spacer and Teflon dielectric in between two layers of different thicknesses of FR4 dielectric are shown in Fig. 3.9(a) and Fig. 3.9(b) respectively while the concerned return loss responses are presented in Fig. 3.10.

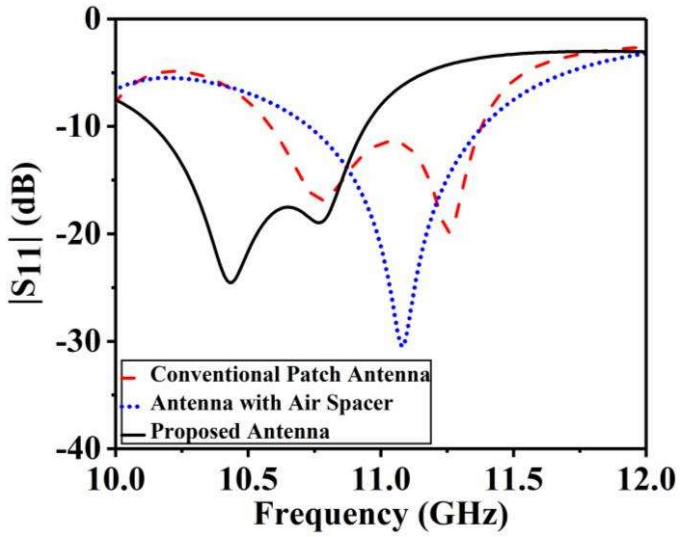

Fig. 3.10. The plot of $|S_{11}|$ (dB) with respect to frequency (GHz) for different cases of the antenna along with the proposed design.

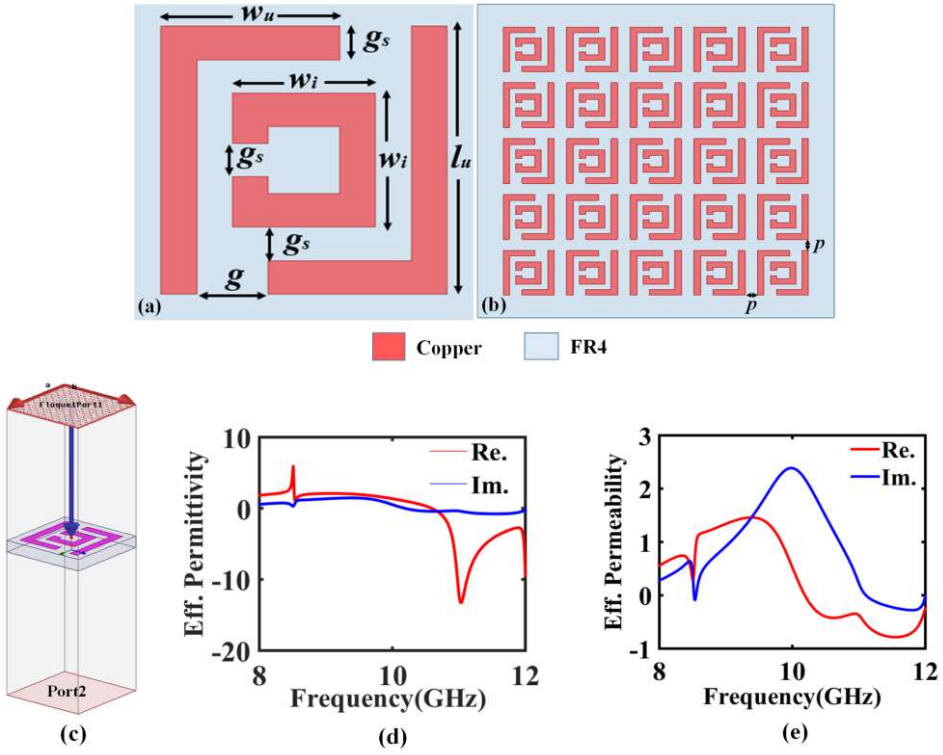

Fig. 3.11. (a) The unit cell of MS (Designed parameters: l_u= 4 mm, w_i= 2 mm, w_u = 2.5 mm, g = 1 mm, g_s = 0.5 mm, p = 1 mm) with (b) 5 × 5 order MS (c) 3D view of unit cell (d) Effective permittivity of unit cell (e) Effective permeability of unit cell.

The MS consists of periodic unit cells with 5×5 order. The unit cell consists of a centered C-type patch surrounded by two L-type patches in the outer side shown in Fig. 3.11(a). The 5×5 order MS and the 3D view of the unit cell are presented in Fig. 3.11(b) and Fig. 3.11(c). The geometrical dimensions of the unit cell and MS are mentioned in Fig. 3.11. The unit cell is excited employing periodic boundary conditions in Ansys HFSS. The primitive electromagnetic properties like effective permittivity and permeability of the concerned MS layer have been studied. The real and imaginary parts of the effective permittivity are shown in Fig. 3.11(d) while the same for effective permeability are illustrated in Fig. 3.11(e). It is clearly observed from Fig. 3.11(d) and Fig. 3.11(e) that the MS layer behaves as a DNG material above 10.4 GHz.

The prototype mentioned in Fig. 3.11 is a left-hand metamaterial (LHM) and the LHM is dominated by metal losses. One way to reduce loss is to use good conductors. On the other hand, it is shown that the losses are closely related to the effective inductance (L) and the effective capacitance (C) in the RLC model of LHM. Increasing the effective inductance to capacitance ratio, L/C, will reduce the losses. LHM materials are suitable for producing narrow beam radiations at far-field as a consequence, engineered structures can be utilized for making small, highly directive, and reconfigurable antennas [15-16]. The 5×5 order of the MS layer with air spacer has been placed over the conventional patch antenna to realize the gain of 7.97 dBi. In addition to that, an impedance bandwidth of 5.77% has been realized at 11.08 GHz. Later, the air space between the conventional patch and the MS layer is again replaced by Teflon dielectric which is represented in Fig. 3.9(b). The optimal gain of 8.17 dBi and fractional bandwidth of 7.66% are achieved simultaneously at 10.44 GHz.

3.3. Simulated Results

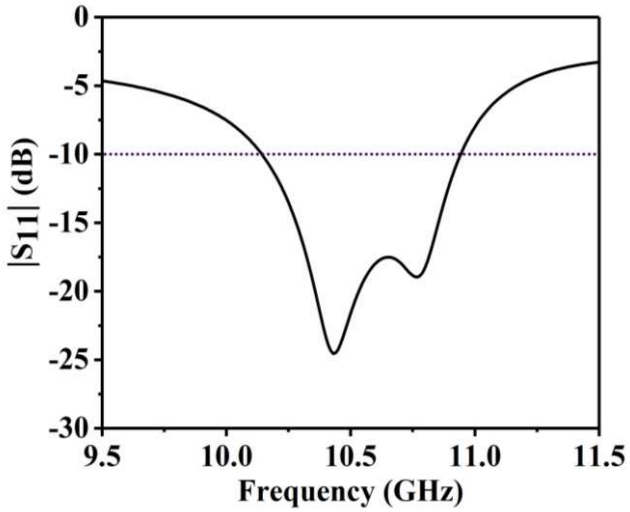

Fig. 3.12. The plot of $|S_{11}|$ (dB) with respect to the frequency (GHz) of the proposed antenna.

The different antenna configurations with respective reflection coefficient characteristics are mentioned in Fig. 3.3 and Fig. 3.10. The proposed conventional fractal patch antenna shown in Fig. 3.1 operates over frequencies ranging from 10.55 GHz to 11.37 GHz with fractional bandwidth of 7.26% with respect to the operating frequency of 11.28 GHz as observed from Fig. 3.10. The maximum return loss of 19 dB has been achieved at 11.28 GHz without incorporating the superstrate configuration. It is clear from Fig. 3.12 that the introduction of metasurface just above the conventional patch results in lowering the operating frequency of the antenna. It is further observed that the proposed antenna operates over the band 10.14 GHz to 10.94 GHz providing fractional bandwidth of 7.66% with respect to 10.44 GHz as evident from Fig. 3.12. The maximum return loss of 24 dB has been achieved at 10.44 GHz. It is further seen that the introduction of a 5×5 order metasurface improves the bandwidth of the proposed antenna.

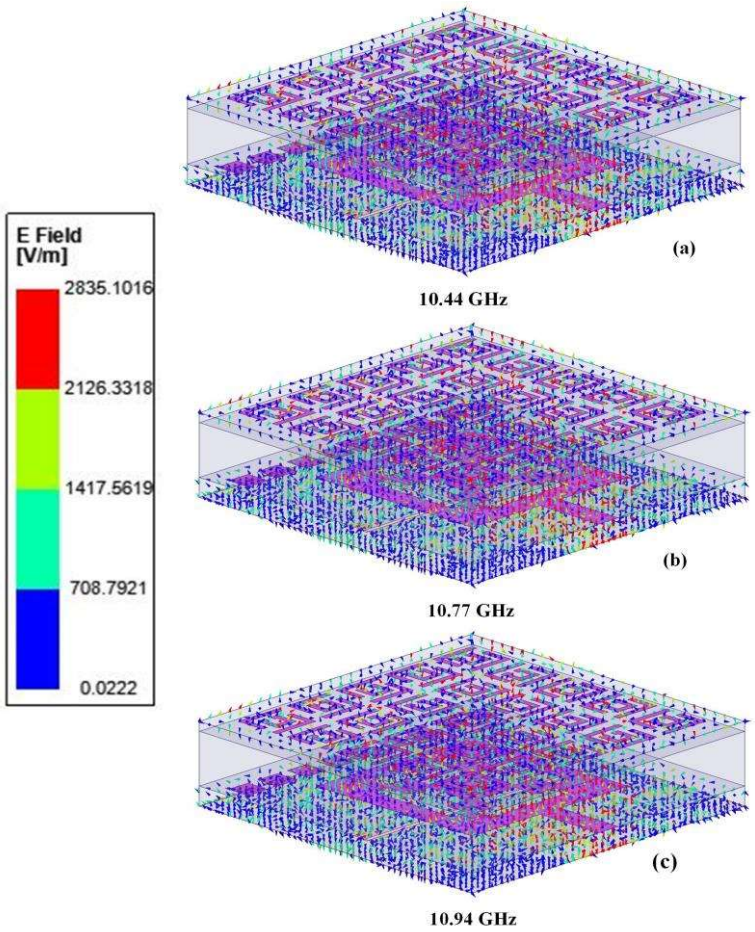

Fig. 3.13. Electric field distributions at (a) top and (b) rear surfaces of the patch (c) 5×5 order metasurface at different operating frequencies within the proposed structure.

The field distributions of the proposed MS-based patch antenna have been studied in Fig. 3.13 and Fig. 3.14. Surface current distribution depicts the flow of current, and the portion of the antenna structure contributing towards the resonance along with the radiating and non-radiating edges. Electric field distribution gives information on the mode of propagation. Electric field lines are most dense around objects with the greatest amount of charge.

The electric field distributions of top and bottom surfaces of the conventional patch antenna at various operating frequencies of 10.44 GHz, 10.77 GHz, and 10.94 GHz are depicted in Fig. 3.13(a) and Fig. 3.13(b) respectively. The electric field distributions in the top

metasurface layer at the aforementioned frequencies are also shown in Fig. 3.13(c). It is observed from Fig. 3.13 that the field distribution is maximum along the edge of the antenna, as well as the intensity of the fields, which is very high among unit cells of the metasurface layer. Furthermore, the electric field is quite intense at the slots present in the ground plane at these three frequencies. The maximum field distribution along the length of the slots has been observed due to inductive and capacitive effects [66-68].

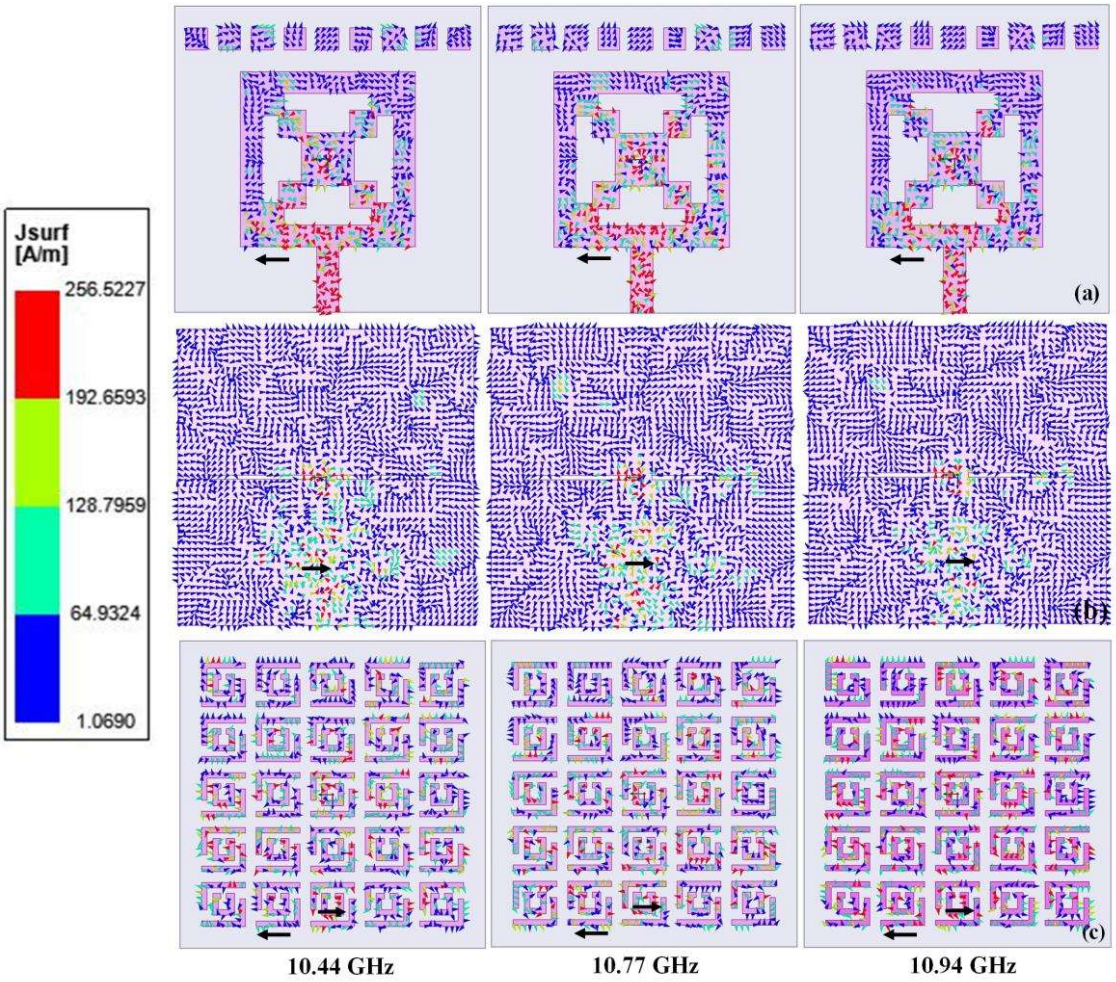

Fig. 3.14. Surface current distributions at (a) top and (b) rear surfaces of the patch (c) 5×5 order metasurface at different operating frequencies within the proposed structure.

The surface currents are also studied simultaneously at the three surfaces of the designed patch antenna at the same frequencies as shown in Figs. 3.14(a) - (c) respectively. It is found that the surface currents are more intense around the antenna aperture and metasurface layer of this proposed antenna at the corresponding frequencies. The current distribution path on the top surface has been increased due to the involvement of the number of unit cell slots on the top surface.

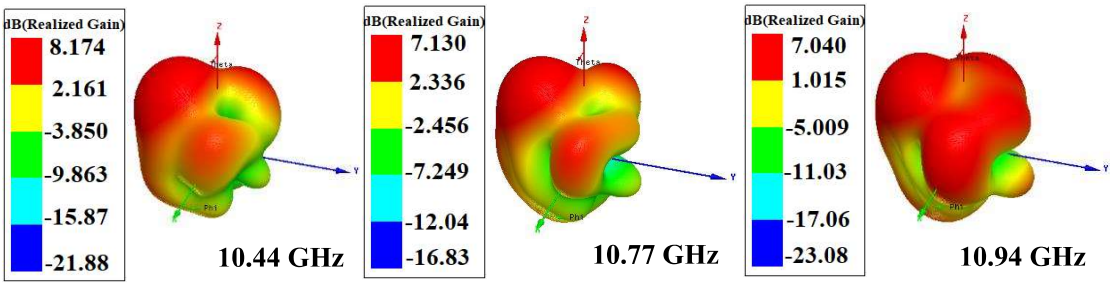

Fig. 3.15. 3D Radiation Pattern at different operating frequencies within the proposed antenna.

The three-dimensional radiation patterns of gain at 10.44 GHz, 10.77 GHz, and 10.94 GHz are shown in Fig. 3.15. It is observed that the realized gain is very high over the entire band of operation of the antenna and the maximum gain of 8.17 dBi has been achieved at 10.44 GHz. The realized gain of the antenna gets enhanced with the change in operating frequency due to the incorporation of more number of unit cells in the metasurface as evident from Fig. 3.13(c) and Fig. 3.14(c).

3.4. Experimental Results

The antenna prototype shown in Fig. 3.1 has been fabricated using LPKF PCB Prototyping Instrument [130]. The top and rear views of the fabricated sample are given in Fig. 3.16(a) and Fig. 3.16(b). The top view of the fabricated MS layer of 5×5 order has been shown in

Fig. 3.16(c). The complete three-dimensional sample is shown in Fig. 3.16(d). The antenna prototype has been tested by Anritsu Vector Network Analyzer (VNA) with model MS 2037C as given in Fig. 3.16(e). Standard calibration techniques have been implemented for the measurement of the return loss profile of the fabricated sample and presented in Fig. 3.16(f) where it is compared with the simulated one. It is found from Fig. 3.16(f) that experimentally measured 10 dB impedance bandwidth has been achieved in the range 9.24-11.25 GHz; thereby providing good matching with the simulated response.

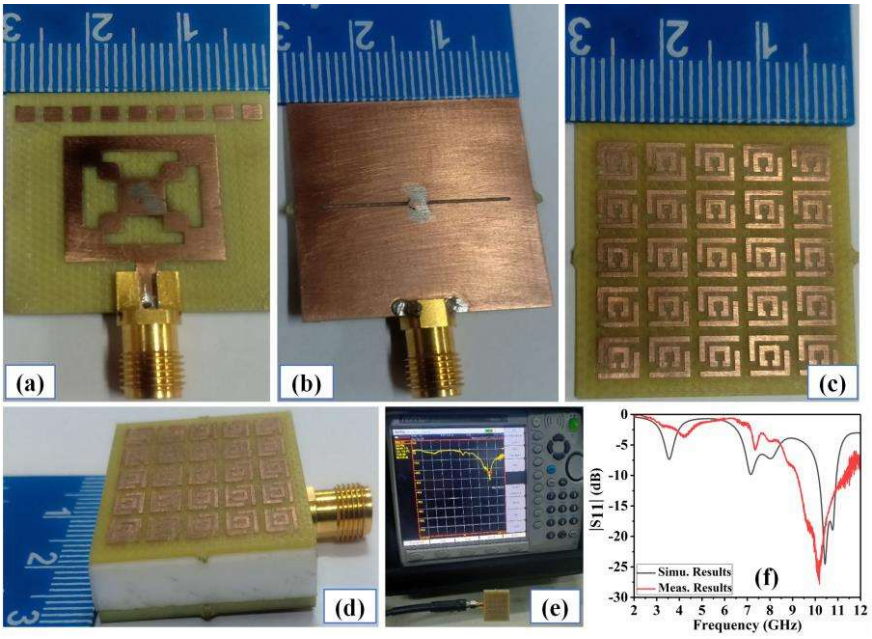

Fig. 3.16. Proposed fabricated structure (a) top view (b) rear view (c) 5×5 order metasurface (d) Three-dimensional view of the proposed antenna (e) $|S_{11}|$ measurement of using VNA (f) Plot of Simulated vs Measured $|S_{11}|$ (dB) with respect to frequency.

The E-plane and H-plane radiation pattern measurements of the fabricated antenna have been performed within the anechoic chamber. The experimental set-up regarding the same has been shown in Fig. 3.17(a) where a wide band horn antenna has been taken as a reference receiving antenna while the fabricated prototype has been considered as the transmitting one.

The antenna under test has been kept in the far-field region as the two antennas are separated by a distance of 1.5 m as shown clearly in Fig. 3.17(a).

Table 3.1. Performance Comparison of Simulated Results with Measured Results of the Proposed Antenna

Results	Bandwidth (GHz)	Return Loss (dB)	Max. Gain (dBi)
Simulated	10.14 -10.94	24	8.17
Measured	9.24-11.25	27	7.57

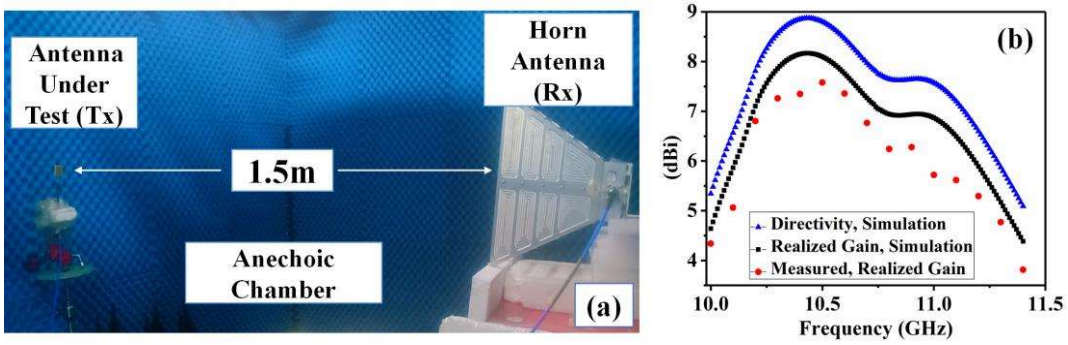

Fig. 3.17. (a) Radiation pattern measurement using anechoic chamber (b) Responses of Simulated vs Measured peak realized gain (dB) with respect to frequency of the proposed antenna.

The far-field antenna gains of the proposed prototype with respect to frequencies are shown in Fig. 3.17(b) where it is compared with the simulated one. In the proposed design, the simulated peak directivity and realized gain are 8.85 dBi and 8.17 dBi respectively. However, the experimentally measured realized gain is 7.57 dBi. Hence, the simulated 3dB directivity bandwidth extends from 10.07-11.31 GHz, which is 11.8% at 10.44 GHz. The simulated and measured realized gains of the proposed antenna are close to each other. It is observed that due to the introduction of metasurface on a simple conventional patch, there is an

improvement of gain in the designed antenna by 7.57 dBi compared to the reference one. The performance study of simulated and experimental results of the proposed antenna is shown in TABLE 3.1 The difference between simulation and design results, may occur due to the fabrication tolerances (may be due to the slight air gap between these dielectric layers at the time of fabrication, soldering between the dielectric substrate and SMA connector or the copper loss of the FR4 dielectric at the time of polishing). In addition, the shift may be due to the insertion loss of the SMA connector.

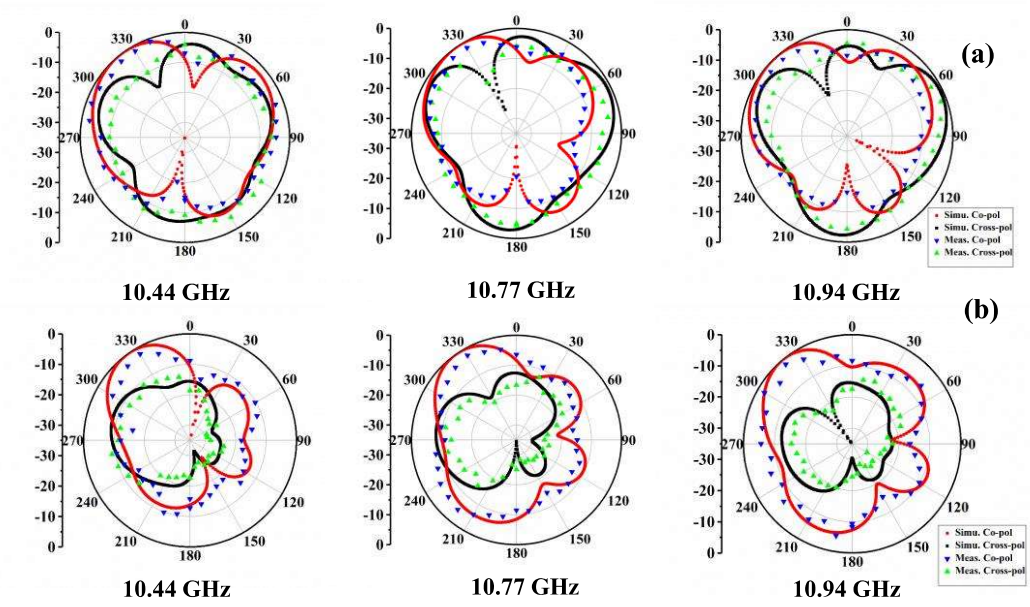

Fig. 3.18. Radiation pattern (a) E-plane Co-polarized and Cross-polarized and (b) H-plane Co-polarized and Cross-polarized at different operating frequencies within the proposed structure.

The radiation pattern characteristics of the proposed antenna along E-plane ($\varphi = 0^0$) and H-plane ($\varphi = 90^0$) have been analyzed and revealed in Fig. 3.18(a) and Fig. 3.18(b) respectively. Unidirectional radiation pattern has been observed both in E-plane and H-plane at 10.44 GHz, 10.77 GHz and 10.94 GHz as evident from the co-polarized radiation patterns. The

unidirectional radiation characteristics at the aforementioned frequencies have been validated by the experimentally measured co-polarized responses as evident from Fig. 3.18. The patterns in the E-plane and H-plane are deviated toward -34^0 and are asymmetric because of the feed offset and the leakage of out of phase fields from few slots either in the ground plane or at the patch. However, the proposed antenna is still acceptable for wireless hand-held devices application for multipath environments having certain distortion. In the E-plane, the measured cross-polarized levels of the proposed antenna remain below 8 dB than that of the co-polarized ones at -34^0 as evident from Fig. 3.18. Furthermore, the measured cross-polarized levels in the H-plane remain below 12 dB from the co-polarized levels at -34^0 in all the operating frequencies. It has been further observed from Fig. 3.18(a) that the main lobe has been directed toward -34^0 for E-plane radiation pattern whereas the next lobe appearing at 52^0 has been considered as side lobe. The simulated and measured normalized values of the main lobe corresponding to E-plane are 0 dB and -1.14 dB respectively at -34^0 while for the side-lobe oriented along 52^0, the respective values are -3.19 dB and -4.72 dB. So, the measured side lobe level (SLL) (-dB) along E-plane is 3.58 at 10.44 GHz. Similarly, for the H-plane radiation pattern, the simulated and measured normalized values of the main lobe are 0 dB and -2.21 dB respectively at -34^0. The side lobe is oriented along 46^0 with simulated and experimental normalized values of -12.4 dB and -12.48 dB respectively as evident from Fig. 3.18(b). Accordingly, the measured SLL (-dB) along H-plane is 10.27 at 10.44 GHz. The SLL values differ slightly at the other frequencies of the operating band as compared to 10.44 GHz. The discrepancies arising among the measured and simulated results may be due to cable and adaptor losses, dielectric loss, and fabrication tolerances during the far-field measurement.

Table 3.2. Comparative Study of the Proposed Antenna with some High-Performance Antennas

Antenna Literature	Overall Dimensions	Operating Frequency (GHz)	Antenna Design Complexity	Antenna Cost	3dB Directivity BW (%)	Gain (dBi)	SLL (-dB) (E-plane)	SLL (-dB) (H-plane)	Cross Polarization Level (-dB) (E-plane)	Cross Polarization Level (-dB) (H-plane)	Radiating Element
Pan *et al.* [141]	$1.3\lambda_0 \times 1.3\lambda_0 \times 0.6\lambda_0$	5	High	High	30	8.2	_	_	25	25	Microstrip-coupled slots
Cao *et al.* [142]	$1.16\lambda_0 \times 1.16\lambda_0 \times 0.26\lambda_0$	5.1	High	High	13	9.3	_	10	20	_	Cross-shaped radiating slot
Kim *et al.* [143]	$1.2\lambda_0 \times 1.2\lambda_0 \times 0.4\lambda_0$	5.75	Very High	High	2.7	6.8	13	16	_	_	A patch
Liu *et al.* [144]	$1.7\lambda_0 \times 1.7\lambda_0 \times 0.02\lambda_0$	10.6	High	Low	_	6.2	14	15	_	_	A patch
Sharma *et al.* [145]	$3.6\lambda_0 \times 3.6\lambda_0 \times 0.14\lambda_0$	13.6	High	Low	14.7	9.1	14	15	20	20	A patch
Zheng *et al.* [146]	$2.8\lambda_0 \times 2.8\lambda_0 \times 0.1\lambda_0$	10.5	Very High	High	16	8.1	14	14	14	14	A patch
Baba *et al.* [147]	$3.1\lambda_0 \times 3.1\lambda_0 \times 0.6\lambda_0$	55.6	Very High	High	16.7	18.8	12	24.5	_	_	Probe feed Patch
Al-Tarifi *et al.* [148]	$20\lambda_0 \times 20\lambda_0 \times 0.4\lambda_0$	14.00	Very High	High	19.3	16.2	11	16	_	_	WR-62 waveguide aperture
Hashmi *et al.* [149]	$1.5\lambda_0 \times 1.5\lambda_0 \times 1.2\lambda_0$	11.10	Very High	High	22	18.2	9.8	16.5	_	_	Defect cavity model
Zheng *et al.* [150]	$2.2\lambda_0 \times 2.2\lambda_0 \times 0.6\lambda_0$	10.80	High	High	16.5	12	11	9	15	15	A patch
Proposed Design	$0.9\lambda_0 \times 0.9\lambda_0 \times 0.29\lambda_0$	10.44	Low	Low	11.8	7.57	3.58	10.27	8	12	Fractal-shaped slotted patch

Table 3.2 compares the performance of the proposed antenna with some of the reported high-performance antennas. From the analysis, it is concluded that the proposed low-profile design exhibits significantly enhanced gain. The proposed antenna has been found to be of low cost

in comparison to the reported ones as evident from Table 3.2. The high-performance antennas in [146]-[150] have achieved superior gain and high value of 3dB directive bandwidth along with reduced SLL and low cross-polarization level as compared to the presented antenna. However, all of these antennas have been designed incorporating larger dimensions printed on higher dielectric constant and low loss substrate. Moreover, the thickness of the antenna profile in all the cases are also very high in comparison to the proposed antenna.

3.5. Concluding Remarks

The metasurface with fractal-shaped slotted patch antenna has been analyzed by varying the periodic unit cell. A layer of teflon, which serves as the superstrate, separates the MS from the typical patch antenna. The gain and impedance bandwidth are more affected due to dielectric via in fractal patch as well as defected ground structure. Good impedance matching over the frequency band is achieved by using the concept of 5×5 order periodic metasurface. The proposed antenna operates at 10.44 GHz frequency with fractional bandwidth of 7.66% and a significantly enhanced gain of 7.57 dBi at the same operating frequency. The simulated and the experimental results validate well; so demonstrating a good antenna performance. The antenna performs a unidirectional radiation pattern in its far-field region. This antenna can be utilized for applications like medical investigation, defense service, satellite communication, etc.